

Visual Pursuit Control based on Gaussian Processes with Switched Motion Trajectories^{*}

Marco Omainka^{*} Junya Yamauchi^{*} Masayuki Fujita^{*}

^{*} *Department of Information Physics & Computing, The University of Tokyo, Tokyo, Japan (e-mail: marcoomainska@g.ecc.u-tokyo.ac.jp).*

Abstract: This paper considers a scenario of pursuing a moving target that may switch behaviors due to external factors in a dynamic environment by motion estimation using visual sensors. First, we present an improved Visual Motion Observer with switched Gaussian Process models for an extended class of target motion profiles. We then propose a pursuit control law with an online method to estimate the switching behavior of the target by the GP model uncertainty. Next, we prove ultimate boundedness of the control and estimation errors for the switch in target behavior with high probability. Finally, a Digital Twin simulation demonstrates the effectiveness of the proposed switching estimation and control law to prove applicability to real world scenarios.

Keywords: Data-based control, Gaussian process, switched control, mobile robots, passivity

1. INTRODUCTION

In robot control and Machine Learning visual sensors are a common tool for recognition tasks since they provide rich information (Quintero et al., 2017; Wahlström et al., 2015). Traditionally they are used for robot manipulators in vision-based control tasks, but recently shift to mobile (aerial) robots due to a wider range of modern applications (Spong et al., 2020): security and surveillance (Pierson et al., 2016), investigation of animal ecology (Shah et al., 2020), bird strike prevention (Paranjape et al., 2017), among others.

The scenario in this paper is the pursuit of a moving target based on visual measurements (Fig. 1), which is a typical problem in the aforementioned applications. Observers to estimate the target pose have been proposed in Quintero et al. (2017); Chwa et al. (2016), but this paper focuses on the passivity-based Visual Motion Observer (Hatanaka et al., 2015) since it simultaneously estimates the rigid body motion while pursuing the target. To avoid the loss of vision to the target, previous research of the authors Omainka et al. (2021); Yamauchi et al. (2021) studied the inclusion of Gaussian Processes (GP), which are Bayesian non-parametric models with many favorable properties: they provide an estimated mean value and measure their own model fidelity in form of a variance function (Rasmussen and Williams, 2006). Furthermore, upper bounds for the error between real and inferred function values based on the distance to training data do exist (Srinivas et al., 2012).

In our previous work (Omainka et al., 2021; Yamauchi et al., 2021) we assumed that targets move according to their environment. A disadvantage about the proposed solutions is that the GP model can express only one particular motion trajectory. This limits real world applicability, since other moving objects in a dynamic environment may

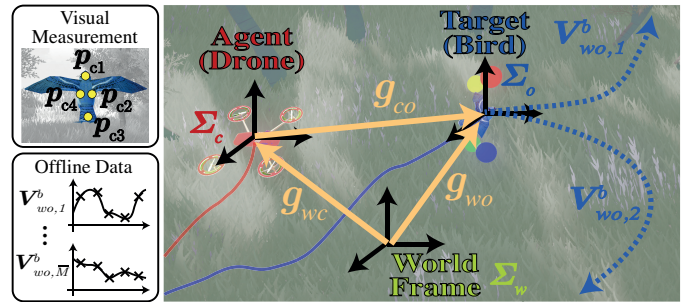


Fig. 1. Pursuit of a *target* (bird) by a camera equipped *mobile robot* (drone) based on visual measurements and motion learning. The target can change its behavior (motion V_{wo}^b) anytime due to external influences.

influence the target behavior. In contrast, Wei et al. (2019) consider multiple trajectories while targets leave and enter a scene. A Dirichlet Process Gaussian Process estimates the probability of a target moving by a certain velocity field, but target motion switching which would require controller switching in our setting is not considered. As such, Umlauf and Hirche (2020) online update the controller, but switching system dynamics are not considered. Similarly, Maiworm et al. (2021) use a model predictive controller with recursive posterior prediction model updates, but switching system dynamics have not been considered.

In this paper, we consider the case of a target switching its motion in a dynamic environment. We propose a method to online estimate the switching based on the GP model uncertainty and accordingly update the controller. The contributions of this paper are as follows: (i) extending the class of motion trajectories to target motion profiles, (ii) proposing a visual pursuit control input with switched GP models and proving stability, (iii) estimating the switching based on the GP variance, (iv) showing applicability to real world scenarios with a Digital Twin simulation.

^{*} This work was supported by JSPS KAKENHI Grant Number 20K14761.

The paper is organized as follows: First, the overall problem is formulated in Section 2. Next, Section 3 introduces the Visual Pursuit System. Section 4 proposes the controller with online switching estimation method, which is then proven to be stable in Section 5. The effectiveness of the proposed controller is proven in a Digital Twin simulation in Section 6. Finally, the conclusion is given in Section 7.

Notation

Vectors/matrices are denoted as bold characters. $\|\cdot\|$ is the Euclidean norm, \mathbf{I}_n the identity matrix of size n and \succ shows positive definiteness of a matrix. $\xi\theta_{ij}$ is the shorthand notation for $\xi_{ij}\theta_{ij}$. Given two vectors $\mathbf{a}, \mathbf{b} \in \mathbb{R}^3$, the wedge-operator \wedge computes $\hat{\mathbf{a}}\mathbf{b} = \mathbf{a} \times \mathbf{b}$ while the vee-operator \vee is its inverse-operation. The operator $\text{diag}(\cdot)$ defines a diagonal matrix with the given elements. $[\cdot]_i$ and $[\cdot]_{i,i}$ denote elements or columns of a given vector or matrix.

2. PROBLEM FORMULATION

2.1 Rigid Body Motion

In this paper we consider the motion of rigid bodies with pose $\mathbf{g} \in SE(3)$ in the special Euclidean group $SE(3) := \mathbb{R}^3 \times SO(3)$. It consists of the position $\mathbf{p} \in \mathbb{R}^3$ and orientation $e^{\xi\theta} \in SO(3)$. The axis-angle pair $\xi\theta \in \mathbb{R}^3$ combines the normalized Euler axis ξ (i.e. $\|\xi\| = 1$) and rotation angle $\theta \in (-\pi, \pi]$. There are multiple representations of the pose \mathbf{g} , but we will focus on the homogeneous representation (Hatanaka et al., 2015)

$$\mathbf{g} = \begin{bmatrix} e^{\xi\theta} & \mathbf{p} \\ \mathbf{0} & 1 \end{bmatrix} \quad (1)$$

and the vector form $\mathbf{g} = [\mathbf{p}^\top \ \xi^\top \theta]^\top$ (Omainka et al., 2021). We consider the scenario of a moving target and camera-equipped mobile robot. Let Σ_w, Σ_c and Σ_o be coordinate frames of the world, camera, and target, respectively. The motion of frame Σ_j with respect to Σ_i is then denoted as

$$\mathbf{g}_{ij} := \mathbf{g}_{wi}^{-1} \mathbf{g}_{wj}. \quad (2)$$

Hence, we formulate the rigid body motion

$$\dot{\mathbf{g}}_{wo} = \mathbf{g}_{wo} \hat{\mathbf{V}}_{wo}^b, \quad \dot{\mathbf{g}}_{wc} = \mathbf{g}_{wc} \hat{\mathbf{V}}_{wc}^b \quad (3)$$

of the target and camera with the body velocity $\hat{\mathbf{V}}^b \in se(3) := \{[\dot{\omega}_0^b \ \mathbf{v}^b] \mid \dot{\omega}^b \in \mathbb{R}^{3 \times 3}, (\dot{\omega}^b)^\top + \dot{\omega}^b = \mathbf{0}, \mathbf{v}^b \in \mathbb{R}^3\}$ where \mathbf{v}^b corresponds to the translational and ω^b to the angular velocity, respectively. The relative rigid body motion (RRBM) from the camera to the target can be obtained from the time derivative of (2) with (3) as

$$\dot{\mathbf{g}}_{co} = -\hat{\mathbf{V}}_{wc}^b \mathbf{g}_{co} + \mathbf{g}_{co} \hat{\mathbf{V}}_{wo}^b. \quad (4)$$

2.2 Switched Target Motion Profiles

The target moves according to the unknown body velocity $\mathbf{V}_{wo}^b = (\mathbf{v}_{wo}^b, \omega_{wo}^b) \in \mathbb{R}^6$ with the following assumption:

Assumption 1. The target moves in a bounded field $D \subset \mathbb{R}^3$, thus, $\mathcal{X} := D \times SO(3)$ is a compact subset of $SE(3)$.

Note that targets naturally move in bounded environments, hence Assumption 1 is non-restrictive. Further, targets are moving under external influences, i.e. terrain and other moving obstacles, and may switch behavior at times.

Previous research (Omainka et al., 2021; Yamauchi et al., 2021) assumed that targets move under the influence of a static environment at which \mathbf{V}_{wo}^b results in only one periodic trajectory. However, this limits the applicability to real scenarios since it does not take into account dynamic environments that may force the target to switch its behavior. Hence, similar to the definition of a position-based velocity field in Wei et al. (2019) we introduce *target motion profiles* $\mathbf{V}_{wo,\psi}^b: \mathcal{X} \rightarrow \mathbb{R}^6$ drawn from a broader set

$$\mathcal{V}^b := \{\mathbf{V}_{wo,1}^b, \dots, \mathbf{V}_{wo,\bar{M}}^b\} \quad (5)$$

where index $\psi \in \Psi := \{1, \dots, \bar{M}\}$ is determined at time $t \in [0, \infty)$ by an unknown switching signal (Liberzon, 2003)

$$s(t): [0, \infty) \rightarrow \Psi \quad (6)$$

resulting in a piece-wise continuous body velocity signal $\mathbf{V}_{wo}^b(t, \mathbf{g}_{wo}) = \mathbf{V}_{wo,s(t)}^b(\mathbf{g}_{wo})$. Note that we exclude infinite switching in finite time cases to prevent Zeno behavior.

Our goal is to follow a moving target (3) under switched motion trajectories (5). It is assumed that the camera knows its pose \mathbf{g}_{wc} , however, since \mathbf{g}_{co} cannot be directly measured, \mathbf{g}_{wo} cannot be calculated from (2) either. A new control law is proposed in Section 4 that improves pursuit under the new target motion profiles (5). We also prove boundedness even if the switching signal (6) is unknown and show a method how it can be estimated online.

3. PRELIMINARIES: VISUAL PURSUIT SYSTEM

3.1 Visual Measurements

In the following we will discuss how the mobile robot gathers information of a moving target through its visual sensor. We assume targets have at least $n_f \geq 4$ feature points (i.e. yellow markers in Fig. 1) which can be extracted by real time Computer Vision techniques such as given in Kane et al. (2020). The positions $\mathbf{p}_{oi} \in \mathbb{R}^3$, $i \in \{1, \dots, n_f\}$ of the detected feature points in target frame Σ_o can be transformed into camera frame Σ_c by a coordinate transformation $[\mathbf{p}_{ci}^\top \ 1]^\top = \mathbf{g}_{co}[\mathbf{p}_{oi}^\top \ 1]^\top$. The positions $\mathbf{p}_{ci} = [x_{ci} \ y_{ci} \ z_{ci}]^\top$ are then projected onto the image plane as $\mathbf{f}_i = \frac{\lambda}{y_{ci}} [x_{ci} \ z_{ci}]^\top \in \mathbb{R}^2$ with $\lambda > 0$ the focal length of the camera (Spong et al., 2020). By stacking all \mathbf{f}_i we obtain the *visual measurement* (Hatanaka et al., 2015, p.105)

$$\mathbf{f}(\mathbf{g}_{co}) = [\mathbf{f}_1^\top \ \dots \ \mathbf{f}_{n_f}^\top] \in \mathbb{R}^{2n_f}. \quad (7)$$

3.2 Visual Pursuit Control

In order to follow the target we have to simultaneously measure its pose $\mathbf{g}_{wo} = \mathbf{g}_{wc} \mathbf{g}_{co}$ from visual information. Since \mathbf{g}_{co} is unavailable, we define an estimate $\bar{\mathbf{g}}_{co}$ of the relative rigid body motion (4) given by the *Visual Motion Observer* (VMO) (Hatanaka et al., 2015, Sec.6)

$$\dot{\bar{\mathbf{g}}}_{co} = -\hat{\mathbf{V}}_{wc}^b \bar{\mathbf{g}}_{co} - \bar{\mathbf{g}}_{co} \hat{\mathbf{u}}_e \quad (8)$$

with the observer input $\hat{\mathbf{u}}_e$. We are interested in driving \mathbf{g}_{co} to a desired pose $\mathbf{g}_d \in SE(3)$ while rendering $\bar{\mathbf{g}}_{co}$ closer to \mathbf{g}_{co} . Thus, let us define the control and estimation errors

$$\begin{aligned} \mathbf{g}_{ce} &:= \mathbf{g}_d^{-1} \bar{\mathbf{g}}_{co}, & \mathbf{e}_c &:= \text{vec}(\mathbf{g}_{ce}) \\ \mathbf{g}_{ee} &:= \bar{\mathbf{g}}_{co}^{-1} \mathbf{g}_{co}, & \mathbf{e}_e &:= \text{vec}(\mathbf{g}_{ee}) \end{aligned} \quad (9)$$

with $\text{vec}(\mathbf{g}) = [\mathbf{p}^\top \ \text{sk}(e^{\xi\theta})^\vee]^\top$ and $\text{sk}(e^{\xi\theta}) = (e^{\xi\theta} - e^{-\xi\theta})/2$. But we cannot compute \mathbf{g}_{ee} due to its dependency on \mathbf{g}_{co} .

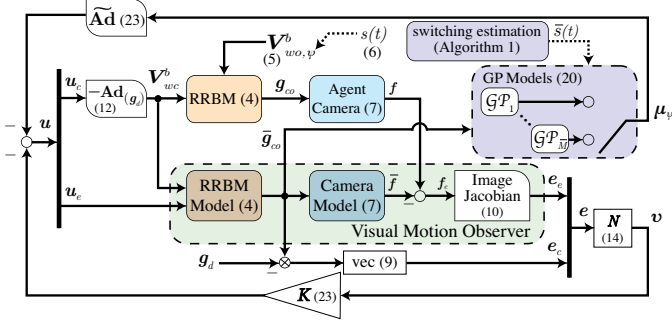


Fig. 2. Block diagram of the visual pursuit system with VMO (8), proposed control law (23), \mathcal{GP}_ψ models (20) and switching estimation Algorithm 1.

Therefore, based on (7) we will compute an estimated visual measurement $\hat{\mathbf{f}}$ from $\hat{\mathbf{g}}_{co}$ and define the visual measurement error $\mathbf{f}_e = \mathbf{f} - \hat{\mathbf{f}}$. Let us make the following assumption: *Assumption 2.* Both the control and estimated rotation error are bounded as $|\theta_{ce}(t)| < \pi/2$, $|\theta_{ee}(t)| < \pi/2$, $\forall t \geq 0$.

This allows us to calculate the estimation error \mathbf{g}_{ee} from

$$\mathbf{e}_e = \mathbf{J}^\dagger(\hat{\mathbf{g}}_{co})\mathbf{f}_e \quad (10)$$

with \mathbf{J}^\dagger the pseudo-inverse of the *image Jacobian* \mathbf{J} (Hatanaka et al., 2015, p.108). Also note that the assumption on θ_{ce} is in our scenario generally satisfied since the mobile robot must be able to move faster than the target for successful pursuit. Now, the time derivative of (9) yields

$$\begin{aligned} \dot{\mathbf{g}}_{ce} &= \hat{\mathbf{u}}_c \mathbf{g}_{ce} - \mathbf{g}_{ce} \hat{\mathbf{u}}_e \\ \dot{\mathbf{g}}_{ee} &= \hat{\mathbf{u}}_e \mathbf{g}_{ee} + \mathbf{g}_{ee} \hat{\mathbf{V}}_{wo}^b \end{aligned} \quad (11)$$

with $\mathbf{u}_c = -\mathbf{Ad}_{(\mathbf{g}_d^{-1})} \mathbf{V}_{wc}^b$. Then, with the *adjoint matrix*

$$\mathbf{Ad}(\mathbf{g}) = \begin{bmatrix} e^{\hat{\xi}\theta} & \hat{\mathbf{p}}e^{\hat{\xi}\theta} \\ \mathbf{0} & e^{\hat{\xi}\theta} \end{bmatrix}, \quad (12)$$

control and estimation error systems $\mathbf{V}_{ce}^b := (\mathbf{g}_{ce}^{-1} \dot{\mathbf{g}}_{ce})^\vee$ and $\mathbf{V}_{ee}^b := (\mathbf{g}_{ee}^{-1} \dot{\mathbf{g}}_{ee})^\vee$, we obtain the overall *error system*

$$\begin{bmatrix} \mathbf{V}_{ce}^b \\ \mathbf{V}_{ee}^b \end{bmatrix} = \begin{bmatrix} \mathbf{Ad}_{(\mathbf{g}_{ce}^{-1})} & -\mathbf{I}_6 \\ \mathbf{0} & \mathbf{Ad}_{(\mathbf{g}_{ee}^{-1})} \end{bmatrix} \mathbf{u} + \begin{bmatrix} \mathbf{0} \\ \mathbf{I}_6 \end{bmatrix} \mathbf{V}_{wo}^b. \quad (13)$$

The input $\mathbf{u} := [\mathbf{u}_c^\top \ \mathbf{u}_e^\top]^\top \in \mathbb{R}^{12}$ is to be designed later in Section 4. Let us also define the stacked error vector $\mathbf{e} := [\mathbf{e}_c^\top \ \mathbf{e}_e^\top]^\top \in \mathbb{R}^{12}$ and output of the error system (13)

$$\boldsymbol{\nu} := \mathbf{N}\mathbf{e}, \quad \mathbf{N} := \begin{bmatrix} \mathbf{I}_6 & \mathbf{0} \\ -\mathbf{Ad}_{(e^{-\hat{\xi}\theta_{ce}})} & \mathbf{I}_6 \end{bmatrix}. \quad (14)$$

The *visual pursuit system* is illustrated in Fig. 2.

4. ONLINE SWITCHING CONTROL LAW

4.1 Gaussian Process Model

Consider noisy measurements of (5) in the form of

$$\mathbf{y} = \mathbf{V}_{wo,\psi}^b(\mathbf{x}) + \boldsymbol{\epsilon}_\psi, \quad \mathbf{x} \in \mathcal{X}, \quad \mathbf{y} \in \mathbb{R}^6 \quad (15)$$

with sub-Gaussian noise $\boldsymbol{\epsilon}_\psi \sim \mathcal{N}(0, \boldsymbol{\sigma}_{n,\psi}^2)$ and standard deviation $\boldsymbol{\sigma}_{n,\psi} := \text{diag}(\sigma_{n,\psi,1}, \dots, \sigma_{n,\psi,6})$. Measurements are stored in M datasets with individually M_ψ datapoints

$$\mathcal{D}_\psi = \{\mathbf{X}_\psi, \mathbf{Y}_\psi\}, \quad \begin{aligned} \mathbf{X}_\psi &:= [\mathbf{x}^{\{1\}} \ \dots \ \mathbf{x}^{\{M_\psi\}}]^\top \in \mathbb{R}^{M_\psi \times 6} \\ \mathbf{Y}_\psi &:= [\mathbf{y}^{\{1\}} \ \dots \ \mathbf{y}^{\{M_\psi\}}]^\top \in \mathbb{R}^{M_\psi \times 6} \end{aligned} \quad (16)$$

On a compact set the *squared exponential (SE)* kernel

$$\mathbf{k}_\psi(\mathbf{x}, \mathbf{x}') = \sigma_{f,\psi}^2 \exp(-\frac{1}{2}(\mathbf{x} - \mathbf{x}')^\top \boldsymbol{\Lambda}_\psi (\mathbf{x} - \mathbf{x}')) \quad (17)$$

computes the correlation between two inputs $(\mathbf{x}, \mathbf{x}')$ and approximates any continuous function arbitrarily precisely (Seeger et al., 2008). It measures properties of (15) together with the symmetric lengthscales matrix $\boldsymbol{\Lambda}_\psi$ and signal variance $\sigma_{f,\psi}$ which are typically obtained by evidence maximization (Rasmussen and Williams, 2006). Finally, the prediction \mathbf{y}^* at test input \mathbf{x}^* is jointly Gaussian distributed with prior mean zero and the posterior mean and variance for every output $i = 1, \dots, 6$ are defined as

$$\mu_{\psi,i}(\mathbf{x}^*) = \mathbf{k}_\psi^\top(\mathbf{K}_\psi + \boldsymbol{\sigma}_{n,\psi}^2 \mathbf{I}_{M_\psi})^{-1} [\mathbf{Y}_\psi]_i \quad (18)$$

$$\sigma_{\psi,i}^2(\mathbf{x}^*) = \mathbf{k}_\psi(\mathbf{x}^*, \mathbf{x}^*) - \mathbf{k}_\psi^\top(\mathbf{K}_\psi + \boldsymbol{\sigma}_{n,\psi}^2 \mathbf{I}_{M_\psi})^{-1} \mathbf{k}_\psi \quad (19)$$

The Gram matrix is computed as $[\mathbf{K}_\psi]_{j,j'} = \mathbf{k}_\psi(\mathbf{X}_\psi^{\{j\}}, \mathbf{X}_\psi^{\{j'\}})$ for $j, j' \in \{1, \dots, M_\psi\}$ and further $[\mathbf{k}_\psi]_j = \mathbf{k}_\psi(\mathbf{X}_\psi^{\{j\}}, \mathbf{x}^*)$. The combined multi-variable Gaussian distribution is then

$$\begin{aligned} \boldsymbol{\mu}_\psi &= [\mu_{\psi,1} \ \dots \ \mu_{\psi,6}]^\top \in \mathbb{R}^6 \\ \boldsymbol{\Sigma}_\psi &= \text{diag}(\sigma_{\psi,1}^2, \dots, \sigma_{\psi,6}^2) \in \mathbb{R}^{6 \times 6} \end{aligned} \quad (20)$$

which we will call the \mathcal{GP}_ψ model for motion profile $\mathbf{V}_{wo,\psi}^b$.

Remark 1. The data (16) is usually hard to obtain online due to real time computation constraints and noisy measurements. However, Omainiska et al. (2021) has proven that we can use the VMO to observe the data. Dividing the dataset into individual target motion profiles has the benefit that conflicts in the data (i.e. crossing points in the target trajectory) can be avoided that would else result in wrong predictions of (18) and higher noise estimates (15).

4.2 Control Law with Switched Motion Trajectories

Consider the common Lyapunov function candidate

$$S_\psi := \frac{1}{2} \sum_{j \in \{c,e\}} (\|\mathbf{p}_{j_e}\|^2 + \text{tr}(\mathbf{I}_3 - e^{\hat{\xi}\theta_{j_e}})) \quad (21)$$

with the time derivative (Hatanaka et al., 2015)

$$\dot{S}_\psi = \boldsymbol{\nu}^\top \mathbf{u} + \mathbf{e}^\top \begin{bmatrix} \mathbf{0} \\ \mathbf{Ad}_{(e^{\hat{\xi}\theta_{ee}})} \end{bmatrix} \mathbf{V}_{wo,\psi}^b. \quad (22)$$

When the target does not move ($\mathbf{V}_{wo,\psi}^b \equiv \mathbf{0}$) the system (13) is passive from input \mathbf{u} to output $\boldsymbol{\nu}$ with respect to the storage function (21). Thus, under Assumption 2 and switched \mathcal{GP}_ψ models (20) we propose the control law

$$\mathbf{u} = -\mathbf{K}\boldsymbol{\nu} - \widetilde{\mathbf{Ad}}\boldsymbol{\mu}_{\bar{\psi}} \quad (23)$$

with $\widetilde{\mathbf{Ad}} := [\mathbf{Ad}_{(e^{\hat{\xi}\theta_{ce}})}^\top \ \mathbf{I}_6]^\top \mathbf{Ad}_{(e^{\hat{\xi}\theta_{ee}})}$ and controller gains $\mathbf{K} = \text{diag}(\mathbf{K}_c, \mathbf{K}_e)$, $\mathbf{K}_c, \mathbf{K}_e \in \mathbb{R}^{6 \times 6}$. The choice of \mathcal{GP}_ψ in (23) depends on the online estimate $\bar{\psi} = \bar{s}(t)$, $\forall t \in [0, \infty)$ of the real switching function (6) and will be discussed next.

4.3 Switching Estimation

In the author's previous work (Omainiska et al., 2021; Yamauchi et al., 2021) a method to adapt controller and communication gains based on the GP uncertainty has been studied. This motivates us in this paper to propose Algorithm 1 to online estimate the switching $\psi = \bar{s}(t)$, $\forall t \in [0, \infty)$ based on the minimum uncertainty

$$\bar{\psi} = \underset{\psi \in \Psi}{\text{argmin}} \frac{\|\boldsymbol{\alpha}_\psi^\top \boldsymbol{\Sigma}_\psi^{1/2}\|}{\bar{\boldsymbol{\Sigma}}_{\boldsymbol{\alpha}_\psi}} \quad (24)$$

Algorithm 1: Switching Estimation of (6)

Output: switching estimate $\bar{\psi}^* = \bar{s}(t)$
Input: Σ_ψ , α_ψ , $\bar{\Sigma}_{\alpha_\psi}$ $\forall \psi \in \Psi$ and $T \in [0, 1)$
Initialize: $\bar{\psi}^*$ from (24)

while controller (23) *running* **do**

 obtain $\bar{\psi}$ from (24);

 if $\|\alpha_{\bar{\psi}^*}^\top \Sigma_{\bar{\psi}^*}^{1/2}\| / \bar{\Sigma}_{\alpha_{\bar{\psi}^*}} > \|\alpha_{\bar{\psi}}^\top \Sigma_{\bar{\psi}}^{1/2}\| / \bar{\Sigma}_{\alpha_{\bar{\psi}}} + T$ **then**

 $\bar{\psi}^* \leftarrow \bar{\psi}$;

 end
end

with the normalization factor $\bar{\Sigma}_{\alpha_\psi} = \max_{\mathbf{x} \in \mathcal{X}} \|\alpha_\psi^\top \Sigma_\psi^{1/2}(\mathbf{x})\|$ since the \mathcal{GP}_ψ models do in general not share equal hyperparameters and noise ϵ_ψ . The design parameter $\alpha_\psi \in \mathbb{R}^6$ specifies the importance of some output dimensions in Σ_ψ on the switching detection. Further, to circumvent abundant switching between \mathcal{GP}_ψ models of approximately equal variance, the constant parameter $T \in [0, 1)$ is introduced in Algorithm 1. At $T = 0$ switching happens immediately, while for higher T switching happens only if the difference in variance is large enough.

5. STABILITY ANALYSIS

In this section we will derive the main theorems of this paper. First, a bound of always using the least accurate \mathcal{GP}_ψ model (worst-case) for unknown switching (6) will be derived. Then, an individual bound for every \mathcal{GP}_ψ model is derived when (6) can be inferred well.

5.1 Ultimate Boundedness for Unknown Switching

Let us assume the following:

Assumption 3. The target motion profiles (5) are bounded, i.e. $\|\mathbf{V}_{wo,\psi}^b(\mathbf{x})\| < \infty$, $\forall \mathbf{x} \in \mathcal{X}$, $\forall \psi \in \Psi$.

We are now ready to state the first theorem about the worst-case scenario when the switching (6) is unknown:

Theorem 1. Suppose that Assumptions 1 to 3 hold. Consider the proposed control law (23) with \bar{M} trained \mathcal{GP}_ψ models (20) of M_ψ datapoints (16) each. Then, the error $\|e\|$ of the error system (13) is uniformly ultimately bounded with regards to arbitrary switching signals (6) and estimate (24).

Proof: Starting from (22) by inserting the control law (23)

$$\begin{aligned} \dot{S}_\psi &= -\nu^\top \mathbf{K} \nu + e^\top \left[\text{Ad}_{(e^{\theta_{ee}})} \mathbf{0} \right] (\mathbf{V}_{wo,\psi}^b - \boldsymbol{\mu}_{\bar{\psi}}) \\ &\leq -\nu^\top \mathbf{K} \nu + \|e_e\| \|\mathbf{V}_{wo,\psi}^b - \boldsymbol{\mu}_{\bar{\psi}}\| \end{aligned} \quad (25)$$

and using Cauchy-Schwarz inequality in the last equation. Since the kernel (17) is continuous, mean (18) is bounded. Together with Assumption 3 it follows that we can find an upper bound $\bar{\Delta}_\mathbf{V} := \max_{\psi, \bar{\psi} \in \Psi} \|\mathbf{V}_{wo,\psi}^b - \boldsymbol{\mu}_{\bar{\psi}}\|$ such that with (14)

$$\begin{aligned} \dot{S}_\psi &\leq -e^\top \mathbf{N}^\top \mathbf{K} \mathbf{N} e + \|e_e\| \bar{\Delta}_\mathbf{V} \\ &\leq -\lambda_{\mathbf{K}} \|e\|^2 + \|e_e\| \bar{\Delta}_\mathbf{V} \end{aligned} \quad (26)$$

where $\lambda_{\mathbf{K}} > 0$ is the smallest eigenvalue of $\mathbf{N}^\top \mathbf{K} \mathbf{N}$. Finally, from $\|e\|^2 = \|e_c\|^2 + \|e_e\|^2$ and quadratic extension

$$\dot{S}_\psi \leq -\lambda_{\mathbf{K}} \|e_c\|^2 - \lambda_{\mathbf{K}} \left(\|e_e\| - \frac{1}{2\lambda_{\mathbf{K}}} \bar{\Delta}_\mathbf{V} \right)^2 + \frac{1}{4\lambda_{\mathbf{K}}} \bar{\Delta}_\mathbf{V}^2 \quad (27)$$

it is shown that the storage function (21) decreases $\dot{S}_\psi < 0$ $\forall \mathbf{g}_{wo} \in \mathcal{X} \setminus \mathbb{B}$, $\forall \psi \in \Psi$ outside the set

$$\mathbb{B} := \{ \mathbf{g}_{wo} \in \mathcal{X} \mid \sqrt{\|e_c\|^2 + (\|e_e\| - c)^2} \leq c \} \quad (28)$$

which forms an ellipse in e with constant $c = \frac{1}{2\lambda_{\mathbf{K}}} \bar{\Delta}_\mathbf{V}$. From (Liberzon, 2003, Theorem 2.1) and the fact that S_ψ is a common Lyapunov function $\forall \psi \in \Psi$, it follows that the error is uniformly ultimately bounded with regards to arbitrary switching signals (6) and converges to ellipse (28). ■

Note that Theorem 1 assures stability for unknown $s(t)$ only with a worst-case bound. We will discuss next a more fitting result when $s(t)$ is known.

5.2 Bound for Known Switching

In order to quantify the \mathcal{GP}_ψ model error $\Delta_{\mathbf{V}_\psi}$ we need to have some prior knowledge about the target motion profiles (5). Hence, we extend Assumption 3 to the following:

Assumption 4. Every target motion profile of (5) has a bounded reproducing kernel Hilbert space (RKHS) norm $\|[\mathbf{V}_{wo,\psi}^b]_i\|_{k_\psi}$ associated with kernel (17) with known hyperparameters for every output $i = 1, \dots, 6$.

This assumption is difficult to verify, however, it only excludes discontinuities and other irregularities within the class (5). We note that even if the overall target body velocity can include discontinuities, Assumption 4 can be still satisfied by the proposed splitting into different target motion profiles $\mathbf{V}_{wo,\psi}^b$ that are continues by themselves.

Lemma 1. Suppose Assumption 4 holds. Then there exists $L_\psi > 0$ such that $\|[\mathbf{V}_{wo,\psi}^b(\mathbf{x})]_i - [\mathbf{V}_{wo,\psi}^b(\mathbf{x}')_i]\| \leq L_\psi \|\mathbf{x} - \mathbf{x}'\|$.

Proof: For the sake of this proof we will use shortened notations $V_i = [\mathbf{V}_{wo,\psi}^b]_i$, $k_{\mathbf{x}} = k(\mathbf{x}, \cdot)$, and $\|\mathbf{x}\|_\Lambda = \sqrt{\mathbf{x}^\top \Lambda_\psi \mathbf{x}}$. From the reproducing property $\langle V_i, k_{\mathbf{x}} \rangle_k = V_i(\mathbf{x})$, $\forall \mathbf{x} \in \mathcal{X}$ we get $|V_i(\mathbf{x}) - V_i(\mathbf{x}')|^2 = |\langle V_i, k_{\mathbf{x}} - k_{\mathbf{x}'} \rangle_k|^2 \leq \|V_i\|_k^2 d_k^2(\mathbf{x}, \mathbf{x}')$ where Cauchy-Schwarz is used for the inequality. We aim to show that the distance over the metric k is upper bounded by $d_k^2(\mathbf{x}, \mathbf{x}') = k_{\mathbf{x}}(\mathbf{x}) - 2k_{\mathbf{x}'}(\mathbf{x}) + k_{\mathbf{x}'}(\mathbf{x}') \leq \sigma_{f,\psi}^2 \|\mathbf{x} - \mathbf{x}'\|_\Lambda^2$ which is easily proven by substituting $r := \|\mathbf{x} - \mathbf{x}'\|_\Lambda$ and (17). We finally obtain $|V_i(\mathbf{x}) - V_i(\mathbf{x}')|^2 \leq L_\psi^2 \|\mathbf{x} - \mathbf{x}'\|^2$ with a Lipschitz constant $L_\psi^2 = \sigma_{f,\psi}^2 \lambda_{\max}(\Lambda_\psi) \|V_i\|_k^2$. ■

Thus, we use (Omainaska et al., 2021, Lemma 4.2) to obtain

$$\|\mathbf{V}_{wo,\psi}^b(\mathbf{g}_{wo}) - \mathbf{V}_{wo,\psi}^b(\bar{\mathbf{g}}_{wo})\| \leq L_{p,\psi} \|\mathbf{p}_{ee}\| + 2\pi L_{\theta,\psi} \quad (29)$$

with Lipschitz constants $L_{p,\psi}$, $L_{\theta,\psi}$. According to Srinivas et al. (2012) we can also state the following:

Lemma 2. Let Assumption 4 hold, then each model error

$$\Delta_{\mathbf{V}_\psi}(\mathbf{x}) = \|\mathbf{V}_{wo,\psi}^b(\mathbf{x}) - \boldsymbol{\mu}_\psi(\mathbf{x})\|, \quad \forall \psi \in \Psi \quad (30)$$

is bounded by a probability $\delta \in (0, 1)$ as

$$\Pr\{\Delta_{\mathbf{V}_\psi}(\mathbf{x}) \leq \|\beta_\psi^\top \Sigma_\psi^{1/2}(\mathbf{x})\|, \quad \forall \mathbf{x} \in \mathcal{X}\} \geq 1 - \delta^6 \quad (31)$$

on the compact set \mathcal{X} where each $\beta_\psi \in \mathbb{R}^6$ is computed as $[\beta_\psi]_i = \sqrt{2\|[\mathbf{V}_{wo,\psi}^b]_i\|_{k_\psi}^2 + 300[\zeta_\psi]_i \log^3((M_\psi + 1)/\delta)}$, based on the maximum information gain $\zeta_\psi \in \mathbb{R}^6$ for $i = 1, \dots, 6$.

Remark 2. It comes natural to assume $\alpha_\psi \equiv \beta_\psi$ as a good candidate in Algorithm 1 since β_ψ details the amount of information in all outputs of the \mathcal{GP}_ψ model. In fact, (24) can then be interpreted as the minimization over the bound (31) for \mathcal{GP}_ψ model error (30) by a certain probability $1 - \delta^6$.

We are now ready to state the main theorem.

Theorem 2. Suppose that Assumptions 1, 2 and 4 hold and the switching (6) with $\psi = \bar{\psi}$ is known. Consider the proposed control law (23) with \bar{M} trained \mathcal{GP}_ψ models (20) of M_ψ datapoints (16) each. Suppose $\tilde{\lambda}_K := \lambda_K - L_{p,\psi} > 0$ with λ_K the minimum eigenvalue of $\mathbf{N}^\top \mathbf{K} \mathbf{N}$ and the Lipschitz constants $L_{p,\psi}, L_{\theta,\psi}$ from (29). Then, the error $\|e\|$ of the error system (13) is uniformly ultimately bounded and converges by a probability $\delta \in (0, 1)$ to an ellipse

$$\mathbb{B}_\psi := \{\forall \mathbf{g}_{wo} \in \mathcal{X} \mid E \leq 0\} \quad (32)$$

$$E := \sqrt{\|e_c\|^2 + \frac{\tilde{\lambda}_K}{\lambda_K} (\|e_e\| - c(\Sigma_\psi))^2} - \sqrt{\frac{\tilde{\lambda}_K}{\lambda_K} c(\Sigma_\psi)}$$

with $c(\Sigma_\psi) = \frac{1}{2\tilde{\lambda}_K} \|\beta_\psi^\top \Sigma_\psi^{1/2}\| + \frac{\pi L_{\theta,\psi}}{\lambda_K}$.

Proof: Since the real \mathbf{g}_{wo} is not available, we have to use its estimation for the \mathcal{GP}_ψ mean prediction $\mu_\psi(\bar{\mathbf{g}}_{wo})$:

$$\dot{S}_\psi \leq -\nu^\top \mathbf{K} \nu + \|e_e\| (\|\mathbf{V}_{wo,\psi}^b(\bar{\mathbf{g}}_{wo}) - \mu_\psi(\bar{\mathbf{g}}_{wo})\| + \|\mathbf{V}_{wo,\psi}^b(\mathbf{g}_{wo}) - \mathbf{V}_{wo,\psi}^b(\bar{\mathbf{g}}_{wo})\|) \quad (33)$$

We used the triangle inequality in (33) and from $\tilde{\lambda}_K > 0$, $\|\mathbf{p}_{ee}\| \leq \|e_e\|$, (29) and (30) the following inequality holds for a probability $\delta \in (0, 1)$ and constant factor $d = 2\pi L_{\theta,\psi}$:

$$\dot{S}_\psi \leq -\lambda_K \|e_c\|^2 - \tilde{\lambda}_K (\|e_e\| - c(\Sigma_\psi))^2 + \tilde{\lambda}_K c(\Sigma_\psi)^2 \quad (34)$$

It follows that the storage function (21) decreases $\dot{S}_\psi < 0 \forall \mathbf{g}_{wo} \in \mathcal{X} \setminus \mathbb{B}_\psi, \forall \psi \in \Psi$ outside set (32) for probability δ . Since $c(\Sigma_\psi)$ is upper-bounded, uniform ultimate boundedness follows analogous to Theorem 1. ■

Remark 3. Theorem 1 proves the existence of a bound for error e for all times, however, the maximum error $\bar{\Delta}_V$ is in practice difficult to calculate. On the contrary, Theorem 2 focuses on providing specific bounds for every $\psi \in \Psi$ individually and by a certain probability. We note that even if $\bar{\psi} = \bar{s}(t)$ is poorly estimated, after an initial convergence period e is bounded between (28) and (32). Further, we note for $T > 0$ in Algorithm 1 Zeno behavior is excluded.

The constant factor in (29) originates from a worst case bound since in general $\xi_{\theta_{wo}} - \bar{\xi}_{\theta_{wo}} \neq \xi_{\theta_{ee}}$. However, in many scenarios rotations are restricted to only one dimension, i.e. the axis of rotation is often fixed as the vertical axis. Let us thus make the following assumption:

Assumption 5. The rotation axis ξ_{wo} is known and fixed.

With Assumption 5 we can fix all initial orientations to $\xi \equiv [0 \ 0 \ 1]^\top$. This simplifies (29) with a Lipschitz constant $\|\mathbf{V}_{wo,\psi}^b(\mathbf{g}_{wo}) - \mathbf{V}_{wo,\psi}^b(\bar{\mathbf{g}}_{wo})\| \leq L_\psi \|e_e\|$ and we obtain:

Corollary 2.1. Let Assumption 5 and the same conditions as in Theorem 2 hold. Then, for $\tilde{\lambda}_K := \lambda_K - L_\psi > 0$, the ellipse (32) is simplified with $c(\Sigma_\psi) = \frac{1}{2\tilde{\lambda}_K} \|\beta_\psi^\top \Sigma_\psi^{1/2}\|$.

Proof: Follows similar to Theorem 2 with the new L_ψ . ■

With Corollary 2.1 the region where $\dot{S}_\psi < 0$ entirely depends on the \mathcal{GP}_ψ model quality. That means, the size of the ellipse (32) depends only on the \mathcal{GP}_ψ variance Σ_ψ and shrinks with more data and a smaller noise variance.

6. SIMULATION

In this section we will illustrate how the proposed control law (23) performs in a Digital Twin simulation¹.

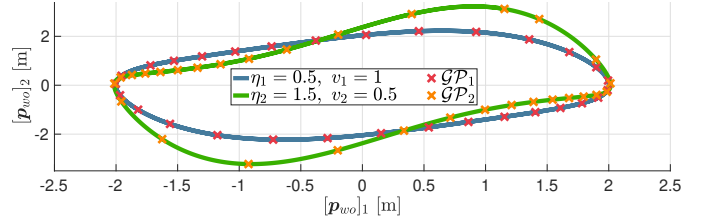


Fig. 3. Bird trajectories resulting from motion profiles (35). The crosses denote the data for two \mathcal{GP}_ψ models (20).

6.1 Setup

The given scenario (Fig. 1) of a target ("bird") and a pursuing mobile robot ("drone") is implemented in Unity, whilst the control input and motion estimation is calculated in MATLAB. Unity and MATLAB communicate over a ROS interface in a Docker-composed network with a message frequency of 50 Hz. For a practical physics simulation, we use the rigid body component of Unity.

The target moves according to the velocity ($\psi = 1, 2$)

$$\begin{aligned} \mathbf{v}_{wo,\psi}^b(\mathbf{g}_{wo}) &= e^{-\hat{\xi}_{\theta_{wo}}} [a_x(\mathbf{p}_{wo}) \ a_y(\mathbf{p}_{wo}) \ 0]^\top \\ \boldsymbol{\omega}_{wo,\psi}^b(\mathbf{g}_{wo}) &= [0 \ 0 \ \frac{d}{dt} \arctan2(a_x(\mathbf{p}_{wo}), a_y(\mathbf{p}_{wo}))]^\top \\ a_x(\mathbf{p}_{wo}) &= v_\psi [\mathbf{p}_{wo}]_2 \\ a_y(\mathbf{p}_{wo}) &= -v_\psi [\mathbf{p}_{wo}]_1 + v_\psi \eta_\psi (1 - [\mathbf{p}_{wo}]_1^2) [\mathbf{p}_{wo}]_2 \end{aligned} \quad (35)$$

with $\eta_1 = 0.5, v_1 = 1$ and $\eta_2 = 1.5, v_2 = 0.5$ resulting in two Van der Pol oscillators as shown in Fig. 3 with the target orientation always heading towards the front path. We learn $\bar{M} = 2 \mathcal{GP}_\psi$ models with $M_\psi = 30$ data points each, where the data is collected according to (15) with noise variance $\sigma_{n,i}^2 = 0.01^2, i = 1, \dots, 6$. Since the target always moves in line of sight we set $\alpha_\psi = [0 \ 1 \ 0 \ 0 \ 0]^\top$ and $T = 0.05$ in Algorithm 1 as the bird forward motion includes the most information for switching detection. The simulation is run for 20s which results in 2 rounds around the trajectory center, while the switching happens at $\mathbf{p}_{wo} = [\pm 2 \ 0 \ 0]$.

The Lipschitz constant $L_\psi \leq \bar{L}$ is approximated by an upper bound $\bar{L} = 8$ for both trajectories. Then, with the controller gains $\mathbf{K}_c = 10\mathbf{I}_6, \mathbf{K}_e = 17\mathbf{I}_6$ and since the target orientation is limited to rotations around the vertical axis, the condition $\tilde{\lambda}_K > 0$ from Corollary 2.1 is satisfied with $\lambda_K = 10$. The rigid body poses are initialized at $\bar{\mathbf{g}}_{co}(0) = ([0 \ 1 \ 0]^\top, \mathbf{I}_3), \mathbf{g}_{wo}(0) = ([-2 \ 0 \ 0]^\top, \mathbf{I}_3), \mathbf{g}_{wc}(0) = ([-2 \ -3 \ 0]^\top, \mathbf{I}_3)$, and $\mathbf{g}_d = ([0 \ 2 \ 0]^\top, \mathbf{I}_3)$. We are interested in the below candidates for the proposed control law (23):

Case 1: Single \mathcal{GP} model trained on full dataset ($M_1 + M_2 = 60$ data points, no \mathcal{GP} switching) from Omainka et al. (2021)

Case 2: Switched \mathcal{GP}_ψ with estimation Algorithm 1

6.2 Results

Figs. 4 and 5 show the simulation results. It is clear that *Case 2* significantly improves the pursuit performance. As such, *Case 1* shows an overall oscillatory behavior (orange trail in Fig. 4) with high error peaks at $t = 11$ s and $t = 12.2$ s in Fig. 5 as a result of \mathcal{GP} misprediction. These are especially prevalent at points where the trajectories overlap,

¹ The code is available at:

<https://github.com/marciska/vpc-switched-motion>



Fig. 4. Simulation snapshot: <https://youtu.be/YxX8FoeyF8g>

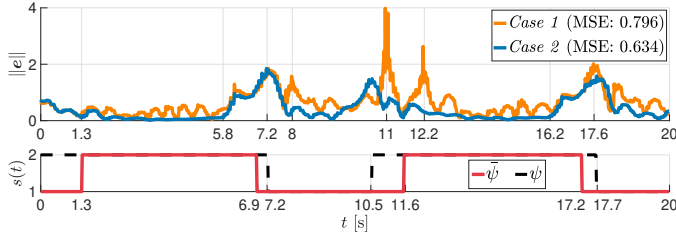


Fig. 5. Top: Comparison of error $\|e\|$. Bottom: Estimated switching $\bar{s}(t)$ (solid) and real $s(t)$ (dashed).

since the velocity (35) on the trajectories Fig. 3 is different and thus the \mathcal{GP} model has to overcome a mismatch in the data. This hypothesis is further strengthened by the fact that the \mathcal{GP} hyperparameters obtained from evidence maximization are significantly larger in the respective outputs than for *Case 2*, and hence the \mathcal{GP} seeks to predict both velocities by a certain trade-off. *Case 2* on the other hand reveals a good performance even when the trajectories overlap, since the distinct motion profiles (35) have been separated into different \mathcal{GP}_ψ models and misprediction can only happen in the case of a bad switching estimate $\bar{s}(t)$. Nonetheless, despite the initial misprediction at simulation start, the results show that Algorithm 1 can sufficiently estimate the switching function (6). Moreover, the oscillatory behavior of *Case 1* is not preserved in *Case 2*.

Overall, *Case 2* (Mean Square Error / MSE: 0.634) shows a 20.35% performance improvement when compared to *Case 1* (MSE: 0.796). In summary, *Case 2* demonstrates that it is important to include target switching behavior in dynamic environments in the control law (23) and that the switching can be well estimated by the proposed Algorithm 1.

7. CONCLUSION

This paper proposes a visual pursuit control law based on a motion observer and switched Gaussian Process models. A new class of target motion profiles is derived that the target can exhibit at times influenced by a dynamic environment. We propose a method to estimate the motion switching based on the GP variance. For every target motion profile a unique error bound is derived. Finally, we show that the proposed control law effectively estimates the switching motion and pursues a target in a Digital Twin simulation.

REFERENCES

Chwa, D., Dani, A.P., and Dixon, W.E. (2016). Range and motion estimation of a monocular camera using static and moving objects. *IEEE Transactions on Control Systems Technology*, 24, 1174–1183.

Hatanaka, T., Chopra, N., Fujita, M., and Spong, M.W. (2015). *Passivity-Based Control and Estimation in Networked Robotics*. Springer.

Kane, G.A., Lopes, G., Saunders, J.L., Mathis, A., and Mathis, M.W. (2020). Real-time, low-latency closed-loop feedback using markerless posture tracking. *eLife*, 9, 1–29.

Liberzon, D. (2003). *Switching in Systems and Control*. Birkhäuser Boston.

Maiworm, M., Limon, D., and Findeisen, R. (2021). Online learning-based model predictive control with gaussian process models and stability guarantees. *International Journal of Robust and Nonlinear Control*, 31, 8785–8812.

Omainka, M., Yamauchi, J., Beckers, T., Hatanaka, T., Hirche, S., and Fujita, M. (2021). Gaussian process-based visual pursuit control with unknown target motion learning in three dimensions. *SICE Journal of Control, Measurement, and System Integration*, 14, 116–127.

Paranjape, A.A., Chung, S.J., Kim, K., and Hyunchul, D. (2017). Robotic Herding of a Flock of Birds Using an Unmanned Aerial Vehicle. *IEEE Transactions on Robotics*, 34, 901–915.

Pierson, A., Ataei, A., Paschalidis, I.C., and Schwager, M. (2016). Cooperative multi-quadrotor pursuit of an evader in an environment with no-fly zones. *2016 IEEE International Conference on Robotics and Automation (ICRA)*, 320–326.

Quintero, S.A.P., Copp, D.A., and Hespanha, J.P. (2017). Robust Coordination of Small UAVs for Vision-based Target Tracking Using Output-Feedback MPC with MHE. In Y. Wang et al. (eds.), *Cooperative Control of Multi-Agent Systems*, 51–83. Wiley.

Rasmussen, C.E. and Williams, C.K.I. (2006). *Gaussian Processes for Machine Learning*. MIT Press.

Seeger, M.W., Kakade, S.M., and Foster, D.P. (2008). Information consistency of nonparametric gaussian process methods. *IEEE Transactions on Information Theory*, 54, 2376–2382.

Shah, K., Ballard, G., Schmidt, A., and Schwager, M. (2020). Multidrone aerial surveys of penguin colonies in antarctica. *Science Robotics*, 5, eabc3000.

Spong, M.W., Hutchinson, S., and Vidyasagar, M. (2020). *Robot Modeling and Control*. Wiley, 2 edition.

Srinivas, N., Krause, A., Kakade, S.M., and Seeger, M.W. (2012). Information-theoretic regret bounds for gaussian process optimization in the bandit setting. *IEEE Transactions on Information Theory*, 58, 3250–3265.

Umlauf, J. and Hirche, S. (2020). Feedback linearization based on gaussian processes with event-triggered online learning. *IEEE Transactions on Automatic Control*, 65, 4154–4169.

Wahlström, N., Schön, T.B., and Deisenroth, M.P. (2015). From pixels to torques: Policy learning with deep dynamical models. *Deep Learning Workshop at the 32nd International Conference on Machine Learning*.

Wei, H., Zhu, P., Liu, M., How, J.P., and Ferrari, S. (2019). Automatic pan-tilt camera control for learning dirichlet process gaussian process (dpgp) mixture models of multiple moving targets. *IEEE Transactions on Automatic Control*, 64, 159–173.

Yamauchi, J., Omainka, M., Beckers, T., Hatanaka, T., Hirche, S., and Fujita, M. (2021). Cooperative visual pursuit control with learning of position dependent target motion via gaussian process. In *60th IEEE Conference on Decision and Control (CDC)*, 2211–2217.